Chemical Engineering Science 294 (2024) 120081

Contents lists available at ScienceDirect

Chemical Engineering Science

journal homepage: www.elsevier.com/locate/ces

A compact 3D printed magnetically stirred tank reactor cascade coupled with a free impinging jet for continuous production of colloidal nanoparticles

Georgios Gkogkos [a], Liudmyla Storozhuk [c,d], Jacopo Piovesan [a,b], Mathew R. Penny [b], Stephen T. Hilton [b], Nguyen Thi Kim Thanh [c,d], Asterios Gavriilidis [a,*]

[a] Department of Chemical Engineering, University College London, Torrington Place, London WC1E 7JE, United Kingdom
[b] UCL School of Pharmacy, University College London, 29-39 Brunswick Square, London WC1N 1AX, United Kingdom
[c] Biophysics Group, Department of Physics and Astronomy, University College London, Gower Street, London WC1E 6BT, United Kingdom
[d] UCL Healthcare Biomagnetics and Nanomaterials Laboratories, University College London, 21 Albemarle Street, London W1S 4BS, United Kingdom

A B S T R A C T

Most colloidal nanoparticle production processes involve more than one step, such as particle nucleation, growth and stabilisation, that often take place at different time scales. Flow chemistry offers an attractive platform for nanoparticle synthesis, as it can provide excellent control of conditions for each individual step. In this work, a free impinging jet reactor (FIJR), known for its rapid mixing capability and fouling-proof operation, is followed by a cascade of 5 miniaturised (3 ml) continuous stirred tank reactors (mCSTR) that provides longer residence time and efficient temperature control for subsequent synthesis steps, while still being resistant to clogging due to active mixing. The small (0.1 mm) diameter nozzle design allowed the FIJR to provide excellent mixing even at relatively low flowrates (2 ml/min/jet). The mCSTR cascade was arranged in a vertical configuration (one tank on top of another), offering a compact design that is simple to use and requiring only one magnetic stirrer. It provided near-ideal macromixing with limited dead volumes and interconnections, as reflected by a residence time distribution comparable with the theoretical one for a CSTR cascade. Most parts of the reactor system were 3D printed with features that facilitated the assembly. The proposed FIJR design overcomes the accuracy limitations of 3D printing by combining it with micromilling to achieve one of the smallest FIJR reported and by allowing for rotation of the nozzles to easily resolve issues with jet alignment. The reactor system was employed for the synthesis of colloidal (~10 nm size) silver nanoparticles via $NaBH_4$ reduction of $AgNO_3$, in a 0.06 g/day scale for 50 min continuous operation and (~6 nm core size) iron oxide nanoparticles via co-precipitation of Fe^{3+}/Fe^{2+}, producing colloidally stable nanoparticles in a 16.1 g/day scale for over 2 h continuous operation.

1. Introduction

Nanoparticles are gaining increasing attention for their remarkable properties that have led to their applications in various domains including catalysis, biomedicine, and environmental applications (McNamara and Tofail, 2017; Mittal et al., 2020; Narayan et al., 2019; Pathakoti et al., 2018). To preserve their properties, nanoparticles typically undergo a stabilisation step involving their coupling with ligands that endow the nanoparticles with colloidal stability (Phan and Haes, 2019). Colloidal nanoparticle synthesis starting from chemical precursors usually involves multiple steps, each with its own characteristic time and individual challenges. To optimise the synthesis of colloidal nanoparticles, each step of the synthetic process towards the final product needs to be considered.

Small scale continuous processes have been found effective for scalable production of high-quality nanoparticles and have the potential to accommodate and optimise each individual stage (Abou-Hassan et al., 2009a, 2009b; Besenhard et al., 2020; Damilos et al., 2021; Panariello et al., 2020; Pinho and Torrente-Murciano, 2020). Fast steps, such as nucleation (a common first step in colloidal nanoparticle synthesis), can benefit from rapid homogenisation of the reactive environment (e.g., heating/cooling or mixing) (Besenhard et al., 2018), while slower steps (usually growth, agglomeration, stabilisation) require good control of residence time distribution and reactive conditions (e.g., temperature) throughout the process in order to obtain a high quality product (Panariello et al., 2018). A recent review has evaluated various continuous flow reactors for nanoparticle synthesis based on these criteria, but predominantly focusing on fouling prevention, which is an important consideration for continuous flow nanoparticle synthesis (Besenhard et al., 2023).

For rapid mixing, only a few reactors can match the efficiency of impinging jet reactors. A Free Impinging Jet Reactor (FIJR) in particular

* Corresponding author.
E-mail address: a.gavriilidis@ucl.ac.uk (A. Gavriilidis).

https://doi.org/10.1016/j.ces.2024.120081
Received 9 November 2023; Received in revised form 28 March 2024; Accepted 1 April 2024
Available online 1 April 2024

(the jets impinge mid-air) is ideal for rapid nanoparticle formation reactions such as precipitation, as it provides fast mixing while also preventing fouling due to a lack of walls in contact with the reaction liquid mixture, and specifically where the liquid streams mix. Due to these characteristics, FIJRs have found applications for nanomaterials synthesis via various rapid reaction routes (Albadi et al., 2020; Baber et al., 2016; Kumar et al., 2013; Proskurina et al., 2019; Sahoo and Kumar, 2021). However, widespread use of FIJRs is hindered due to specific limitations. FIJRs can only operate efficiently within certain operating windows of flowrate, the lower limit being the minimum jetting velocity (minimum velocity required for the transition from droplet formation to jetting (Clanet and Lasheras, 1999), while the upper limit is dictated by instabilities of the liquid sheet that lead to its disintegration, resulting in reduced mixing efficiency (Abiev and Sirotkin, 2020; Baber et al., 2016; Kumar et al., 2013; Li and Ashgriz, 2006). Furthermore, FIJRs can only control the reaction during the initial mixing, and thus cannot provide residence time for multiple synthetic stages or for syntheses requiring longer time, which is often the case in the synthesis of functional nanomaterials. The operation limits of FIJRs can be potentially extended by using nozzles of different size based on Weber number similarity, or by altering the liquid properties by introducing surfactants (Erni and Elabbadi, 2013). For additional control over residence time, they can be coupled with stirred tanks (as in continuous crystallisers (Tacsi et al., 2021), allowing control in both nucleation and growth steps of crystals.

Continuous stirred tank reactors (CSTRs) have been gaining renewed popularity in the fine chemicals industry where solids handling is required (e.g., crystallisation) (Cherkasov et al., 2022). There are also some applications of CSTRs for nanoparticle synthesis (Asimakidou et al., 2020; Deshpande and Kulkarni, 2018). A recent miniaturisation trend on CSTRs led to the development of small scale CSTR cascades that offer tuneable residence time, improved residence time distribution compared to a single tank reactor and reasonable solids handling due to active stirring and relatively large volume/surface ratio (Chapman et al., 2017; Mo and Jensen, 2016). Such miniaturised CSTR (mCSTR) cascades present a promising alternative for nanomaterials synthesis (Lignos et al., 2020, 2021). However, due to their volume/surface ratio, they may still not be able to compete with micro/millifluidics in terms of mixing and heat transfer rate. Recent work has shown that in a small volume, magnetically agitated vertical multi-unit stirred reactor, micromixing could be improved by the addition of premixing units (Chen et al., 2023).

In this work, a FIJR is combined with a mCSTR cascade in a compact configuration by minimising interconnections between the stirred tanks. The proposed modular design aims to enable low cost, rapid manufacturing and easy deployment of the reactor in a laboratory setting by using commercial 3D printing technology and to be used at small scales (e.g., to accelerate materials discovery by providing ideal reaction conditions), while also potentially allowing quick upscaling of colloidal nanoparticle synthesis without compromising the quality of the product. The combination of the FIJR with mCSTRs provides various advantages. The FIJR can enhance micromixing for rapid reaction stages where fast mixing is critical (such as precipitation), while the mCSTR cascade targets the extension of residence time in a controlled and homogeneous environment to allow the completion of slower reaction stages. Furthermore, both components are designed to offer less confined environments compared to conventional microfluidic/millifluidic reactors (which usually involve a T-, cross, or Y- mixer followed by a flow channel), allowing improved fouling and clogging resistance.

2. Materials and methods

2.1. Chemicals

For the residence time distribution study, methylene blue (solid powder obtained from Sigma Aldrich) solution (0.0085 mg/ml) was used giving a peak absorbance of 0.8 a.u. at 654 nm for 1 cm optical path length. For the silver nanoparticle (AgNP) synthesis, the silver precursor solution was prepared by diluting a silver nitrate 10 mM stock (Fluka) to a final concentration of 0.2 mM with deionised (DI) water. Sodium borohydride ($NaBH_4$) solution was prepared by dissolving solid $NaBH_4$ (96 %, obtained from Fischer Scientific) in chilled (0 °C, stored in ice) sodium citrate (0.3 M) solution (pH = 12, achieved by titrating with NaOH 2 M stock). The low temperature and high pH aimed to prevent hydrolysis of $NaBH_4$. Aged (1 d) aqua regia was used to clean the reactor after AgNP synthesis. For the iron oxide nanoparticle (IONP) synthesis, ferric chloride and ferrous chloride (Sigma Aldrich) were dissolved in DI water, producing a precursor solution of 0.1 M (total iron concentration) with $Fe^{3+}/Fe^{2+} = 2$. This iron ion ratio was chosen to favour the production of magnetite (Jolivet et al., 2004). Tetraethylammonium hydroxide (TEAOH) 0.57 M was used by diluting 20 % (w/w) stock solution (Sigma Aldrich) in DI water. HCl 1 M (Fischer Scientific) was used for removing any reactor fouling by iron oxide nanoparticles.

2.2. Reactor manufacturing and assembly

The custom-made reactor parts were designed in Autodesk Fusion 360 (2021) and were directly 3D printed with a Form 3 Stereolithography (SLA) 3D printer (Formlabs) in high temperature resin (HT V2, Formlabs). All parts were fitted in the printing plate (see Figure S1) and printed simultaneously overnight. A micromilling machine (Minitech MiniMill3) with a 0.1 mm drill bit was used to open the orifices of the FIJR nozzles, since the nozzle diameter is a critical dimension for the proper design and operation of the FIJR. More details on 3D printing settings and post processing are available in the SI, section S1. The standard reactor configuration consists of a FIJR module, 5 mCSTR modules, an adapter to hold the FIJR on top of the mCSTR cascade and a base module to keep the whole reactor system in place (all were 3D printed), as well as two preheating coils (each with 2 m of 1 mm internal diameter (ID) PTFE tube coiled on a 17 mm outside diameter (OD) cylindrical PVC scaffold), which were attached on the reactor base via zipties. The mCSTRs were assembled in a vertical orientation via threads embedded on the tank walls. This facilitates a compact assembly in which the bottom wall of one tank doubles as the top wall of the next one. Sealing between the tanks required the use of VITON O-rings due to the rigid material of choice. The assembly of the main reactor parts is depicted in Fig. 1a in an exploded view and in Fig. 1b as assembled, while in Fig. 1c as a cross section showcasing the internal features. Each mCSTR provided ~ 3 ml (3.05 ml, 16 mm diameter and 16 mm height) of volume when using a 4.5 mm × 12 mm cylindrical stir bar with hemispherical edges (see Fig. 1). The top mCSTR was open (i.e., it did not have a top wall), in order to receive the outlet stream from the FIJR. Photographs and further information on the reactor parts, manufacturing process and assembly can be found in the SI, section S1. In addition to the mCSTR cascade, a coiled capillary (PTFE, 1 mm ID, 15 ml total volume) was used (after the mCSTRs) to provide additional residence time for the iron oxide nanoparticle synthesis. It is worth mentioning that the use of the resin 3D printing technology, while allowing for rapid prototyping for geometry optimisation and facile manufacturing of the reactors (both FIJR and the mCSTRs with threads embedded in each tank), introduces the risk of material incompatibilities. Assessment of chemical compatibility with the chemicals used in the nanoparticle syntheses (see SI, section S4) showed good resistance of the resin employed for making the reactor, even for harsh chemicals.

2.3. Reactor operation

In normal operation the fluid flowed from the top to the bottom tank. Two pumps were required to supply the reactants, while an additional peristaltic pump (Masterflex, L/S) at the outlet of the last (bottom) mCSTR, typically operating at the same flowrate as the sum of the inflow pumps, allowed the control of the outflow and kept the fill level of the

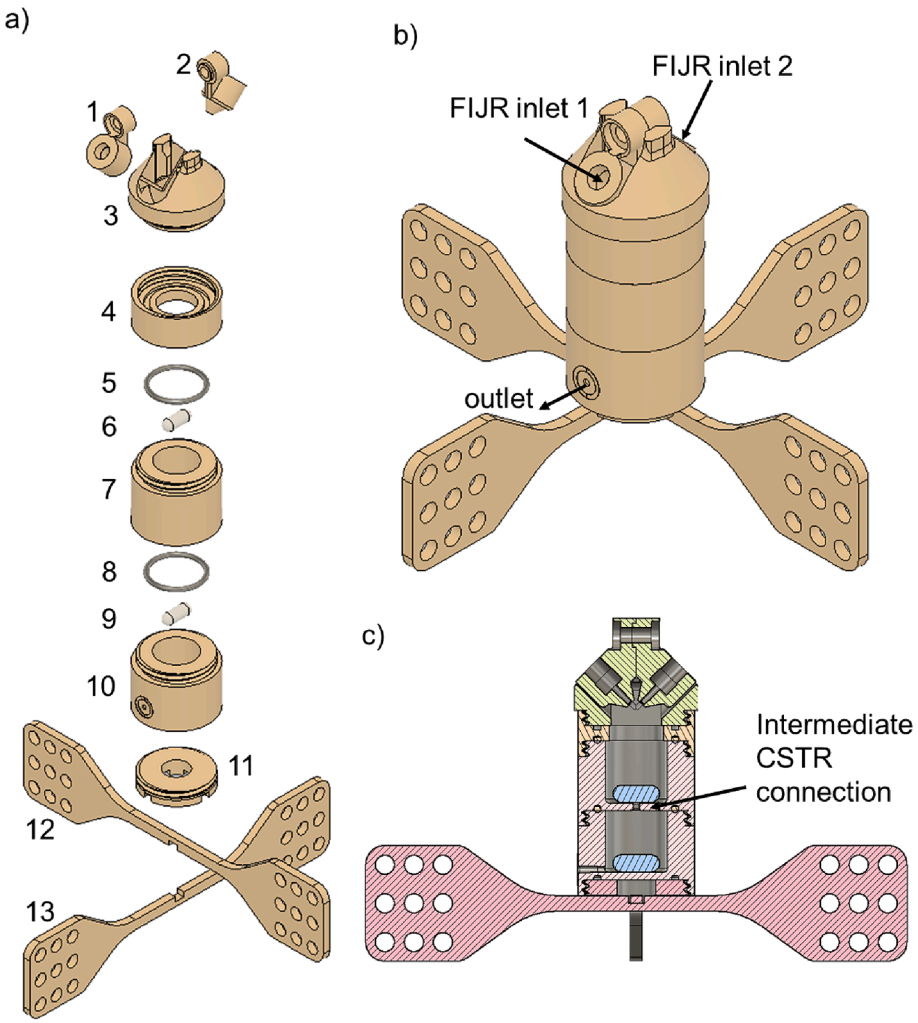

Fig. 1. Assembly of the 3D printed miniaturised continuous stirred tank reactor (mCSTR) cascade parts with the free impinging jet reactor (FIJR). a) Exploded view, 1,2: FIJR nozzles, 3: FIJR holder, 4: thread adaptor, 5,8: VITON O-rings, 6,9: PTFE coated magnetic stir bars, 7: mCSTR module. 10: bottom mCSTR module, 11: primary base module, 12,13: secondary reactor base modules. b) Isometric view of the reactor assembly. c) Cross section of the reactor assembly showcasing internal configuration. Two mCSTR modules are shown, but multiple modules can be used depending on the application.

top mCSTR constant while enabling the connection of the mCSTR cascade with subsequent process steps or sample storage vessels. During nanoparticle synthesis the reactants were fed to the reactor either via syringe pumps (Harvard, PHD Ultra) for the AgNP synthesis, or via continuous piston pumps (Global FIA, milliGAT) for the IONP synthesis.

For the reactor startup, the mCSTR cascade needed to be primed, i.e. the mCSTRs and their intermediate connections needed to be completely filled with liquid. This was done manually using a disposable plastic syringe connected at the outlet of the bottom mCSTR to fill all the mCSTRs with the solvent used in the process (in this work only DI water). This way the mCSTR cascade filled from bottom to the top, taking advantage of buoyancy to remove bubbles. Bubbles were not reintroduced when the flow was reversed during normal operation, due to the open nature of the FIJR, where the reactant streams were introduced.

In a standard configuration, temperature control was achieved by partially submerging the reactor into a magnetically stirred heating water bath, including the preheating coils and only leaving the FIJR part out of the heating fluid as shown in Figure S6. Heating and magnetic stirring was provided by a hotplate/stirrer (IKA, IKAMAG 700). With the vertical orientation of the mCSTRs, the same magnetic stirrer provided stirring for up to five 3 ml mCSTR modules in addition to stirring the heating fluid. A picture of the assembled system is shown in Figure S6.

2.4. High speed imaging

High speed imaging was employed for evaluation of the impinging jet flow hydrodynamics. A high-speed camera (Photron, Mini AX100) fitted with a 5x magnifying lens was used to monitor the flow pattern during the operation of the FIJR. The camera was placed perpendicular to the impingement plane to capture the liquid sheet shape. The impinging jets were formed by feeding DI water continuously to the FIJR via MilliGat pumps. The camera was operated at 11,000 frames per second which allowed the capture of the hydrodynamic flow pattern, as well as oscillations occurring during the pump operation.

2.5. Residence time distribution

The residence time distribution (RTD) of the mCSTRs was obtained with a step infusion of an optical tracer method adapted from (Rossi et al., 2017). In these experiments, the concentration of an optical tracer (methylene blue) was recorded over time at the outlet of the reactor by measuring the UV–Vis absorbance of the outlet stream with a UV–Vis spectrometer (Ocean Optics, USB2000) using a deuterium-tungsten light source (Ocean Optics, DT-mini-2-GS). An abrupt switch from a clear inlet stream (DI water) to a methylene blue (0.0085 mg/ml) solution was done via a switch valve (IDEX, 4 port manual switch valve),

corresponding to a step infusion of the tracer. An extensive description of the experimental setup, procedure and data processing can be found in the SI, section S3.

2.6. Nanoparticle characterisation

Dynamic Light Scattering (DLS) (Beckman Coulter, Delsa Max Pro) was used to measure the average hydrodynamic diameter of the produced IONPs assuming a normal distribution, while regularisation analysis was used to obtain a particle size distribution. For DLS measurements, the IONP samples were diluted 50 times with DI water to avoid multiple scattering.

X-ray diffraction (XRD) (Malvern, PanAlytical X'Pert Pro, with Co Kα radiation ($\lambda = 1.789$ Å)) was used to verify the produced iron oxide phase. For XRD, IONPs were magnetically separated (assisted by adding NaCl (10 mg/ml), washed with DI water and dried in a fume hood.

UV–Vis spectroscopy (Ocean Optics, QE Pro) was used to verify the formation of silver nanoparticles by identifying the characteristic absorbance peak attributed to surface plasmon resonance (SPR).

Transmission Electron Microscopy (TEM) imaging (JEOL 1200 EX operated at 120 kV acceleration voltage) was used to characterise the particle morphology and obtain particle size and particle size distributions. Samples of silver nanoparticles were deposited as prepared on carbon coated copper grids, while iron oxide nanoparticles were diluted 1/100 with DI water to obtain clearer images.

3. Results and discussion

3.1. Reactor system design

The reactor system described in this work (Fig. 2) combined various components, capitalising on the advantages of each; the FIJR provided rapid initial mixing without any particle/wall interaction due to the wall-free environment, which was expected to prevent issues with fouling and clogging during fast particle formation. To compensate for the very short residence time of the FIJR, its outlet stream was fed directly in the first tank of a mCSTR cascade which ensured that the reactive mixture stayed homogenous, and any particles contained, remained dispersed via active mixing even before being stabilised. The mCSTR system can provide control over the residence time by tuning the tank volume and residence time distribution by changing the number of stirred tanks. Furthermore, the small tank diameters, combined with efficient millifluidic preheaters, enabled highly accurate temperature control. The temperature homogeneity was ensured by measuring the temperature in multiple points in the heating bath as well as in the first mCSTR using a thermocouple during operation of the reactor with water at 4 ml/min. The temperature difference between the heating fluid and the first mCSTR was < 3 °C. The design of the individual components is

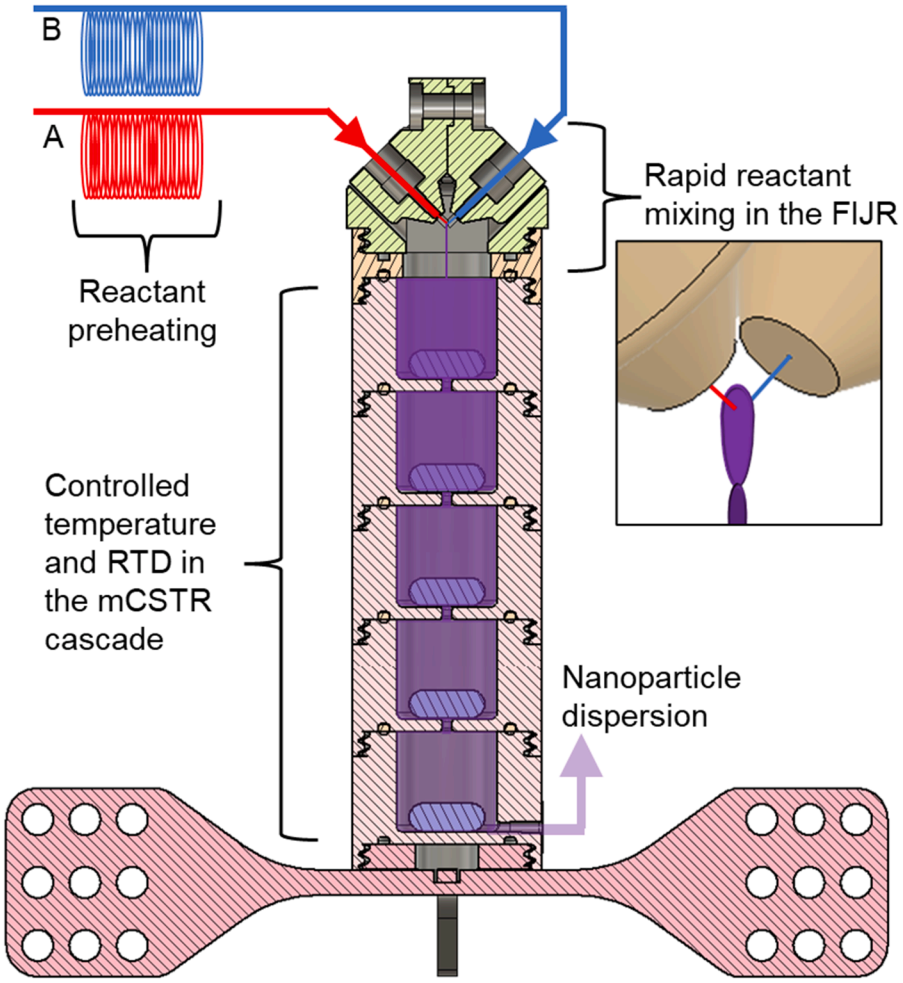

Fig. 2. Schematic of the reactor system with 5 mCSTR modules showcasing the initial mixing via the FIJR, the liquid filled sections and reactant flow in the vertical mCSTR cascade.

discussed in the next subsections.

3.1.1. Design of the FIJR

A proper choice of design parameters was necessary to enable the efficient operation of the reactor system. For a FIJR, efficient mixing requires sufficient jet momentum which is usually achieved at high flowrates. With the reactor initially being targeted towards smaller scale production (to allow its application for synthesis optimisation and material discovery) the orifice diameter was reduced to 100 μm (leading to a similarly small jet diameter), allowing high momentum jet formation at flowrates as low as 1.5 ml/min/jet. For comparison, during preliminary studies it was found that the minimum flowrate for jet formation for a 250 μm nozzle was $>$ 5 ml/min, while typical FIJR operation ranges from 10 to 20 ml/min/jet (Baber et al., 2016; Sahoo and Kumar, 2021). Thus, FIJR downsizing can be beneficial for reducing the cost and waste production of process development. In addition to the nozzle diameter, the other important FIJR design parameter is the impingement angle. Large impingement angles lead to reduction of mixing efficiency, as well as deviation from a planar, leaf shaped impingement zone (Kumar et al., 2013) which is essential to direct the FIJR outlet stream into the mCSTR cascade. However, with increasing impingement angle, the x-component of the jet velocity (perpendicular to the impingement plane) increases, which has been shown to be more important for mixing compared to the total velocity (Sahoo and Kumar, 2021). In the present design, an impingement angle of 90° was chosen as a compromise between retaining well defined and directed leaf-shaped liquid sheet at the impingement plane, and a satisfactory x-component of jet velocity, even at relatively low flowrates. A critical FIJR manufacturing challenge, arising especially in small scales, is alignment of the free jet flows. This was resolved by allowing a rotational motion in the push-fit joint between the jet nozzles, as described in SI, section S1.

3.1.2. Design of the vertical mCSTR cascade and evaluation of magnetic stirring stability

The vertical orientation of the mCSTR cascade brings several advantages mentioned earlier, including a compact design, operation of multiple reactors with a single magnetic stirrer and easy gas bubble removal. Another benefit of the vertical configuration is the axisymmetric placement of the flow ports between tanks, directly below the centre of the stir bar (which covers a large portion of the tank diameter), requiring the fluid to pass through an intensely mixed area to exit the stirred tank. This aims to promote good mixing behaviour, avoiding bypassing and dead volumes. The design also allows for negligible volume of the connection ports between the mCSTRs, which is desirable for mCSTR cascades (Lignos et al., 2020; Mo and Jensen, 2016). Properly sizing the ports requires a balance between volume minimisation, mitigation of pressure drop, resistance to fouling and prevention of backmixing. Increasing the port diameter is expected to decrease pressure drop and reduce the chances of clogging. However, a very large port diameter combined with short interconnection length can lead to increased backmixing. In our design, the port volume was 0.2 % of the mCSTR volume, and its diameter 10 % of the tank diameter. The effectiveness of this design (as well as an alternative design with multiple, larger outlets) is further discussed in section 3.3 and SI, section S6.

An additional challenge arising from the vertical configuration of the mCSTRs concerns the simultaneous magnetic agitation in all mCSTRs. The stirring of multiple mCSTRs with a single rotating magnetic field becomes increasingly challenging with increasing distance of the stir bar from the stirrer, due to weakening of the magnetic attraction between them (magnetic coupling force). It was expected that after a certain distance, the attraction would not be sufficient to initiate (or sustain) the stir bar rotation, leading to instability. Important parameters for stirring stability are the tank and stirring configuration (relative tank and stir bar dimensions and number of tanks), the magnetic stir bar material, the fluid viscosity and the temperature. In our design, cobalt-samarium rare earth magnetic stir bars were primarily used, as they were proven to be responsive at distances over 15 cm above the rotating magnetic field created by conventional hotplates/magnetic stirrers. The stability of magnetic stirring was assessed as described in SI, section S5. To set some guidelines for sizing the mCSTRs regarding magnetic stirring, a series of experiments was performed by varying the distance between the stir bars (which is equivalent to the tank height), and the number of stir bars (which is equivalent to the number of simultaneously stirred mCSTRs in the cascade). It was found that when more than one stir bar rotated simultaneously, instabilities would develop mostly for the top stir bar, when increasing the stirring speed beyond a certain value that depended on both the tank height and the number of tanks; increasing both parameters decreased the maximum stirring speed where stable stir bar rotation was attainable. The various types of instabilities observed are described in detail in SI, section S5, and the results of the stability study are summarised in Table S1. The tank height was found to affect the maximum number of tanks that could be simultaneously stirred (increase of tank height led to a decrease in maximum usable tank number). Special mention should be given to the interaction between the magnetic stir bars (especially when strong, rare earth stir bars are used). When in close proximity (i.e., when the tank height was small), attraction between the magnets led to early onset of instabilities, preventing the stable stirring of the reactor. Thus, the maximum tank height in a vertically oriented, magnetically stirred mCSTR cascade is limited for a given stir bar size, by the desired number of stirred tanks; the minimum tank height is primarily dictated by the interaction between the stir bars.

From the tested configurations, the one with 5 stages and distance between stir bars of 19 mm (Table S1) was used for the rest of the study, as it provided the maximum number of mCSTRs and was able to operate at relatively high stirring speeds (up to 800 rpm). It should be noted that when this configuration was used above a 6th larger (6 mm $\times$ 25 mm) magnetic stir bar (to stir the heating fluid), the simultaneous rotation of all 6 stir bars could be retained for stirring speeds of up to 750 rpm at room temperature (22 °C) or 600 rpm at 70 °C. Since only minimum influence of the temperature in the magnetisation of cobalt-samarium rare earth magnetic stir bars is expected, the difference was attributed to variation of fluid viscosity with temperature. Operating at a lower viscosity medium, vibrations and oscillations occurring during stirring were not effectively dampened, leading to instability that may disrupt smooth operation of the mCSTR cascade. Despite this limitation, the mCSTR cascade operation was stable when fully primed and operated within the defined stirring speed limits.

3.2. FIJR flow regime evaluation

An estimate of the mixing quality provided by the FIJR was obtained by evaluating the shape/flow pattern of the liquid sheet produced at the impingement plane. It has been shown (Baber et al., 2016) that the mixing efficiency of a FIJR can be correlated with the jet Weber number, increasing with an increase in Weber number up to a maximum value after which the efficiency starts to slowly decrease. This behaviour has been associated with flow instabilities arising at high Weber numbers that lead to premature breakage of the liquid sheet into droplets and ligaments that contain partially mixed reactants, leading to lower overall mixing efficiency.

The flow patterns of the liquid sheet produced by the FIJR operated at varying flowrates (i.e., Weber numbers) were captured with a high-speed camera, and are shown in Fig. 3. From Fig. 3a to 3d the expected behaviour is observed with a transition from the “liquid chain” flow pattern in (a), to the closed rim in (b) and its expansion (c), and finally to instability (d). The closed rim patterns have been shown to provide the optimal mixing behaviour in FIJRs. To compare with similar systems reported in the literature, the Weber number was calculated using the horizontal velocity component only (which was shown to play the most important role in mixing efficiency (Sahoo and Kumar, 2021)), to take into account the difference between the impingement angles :

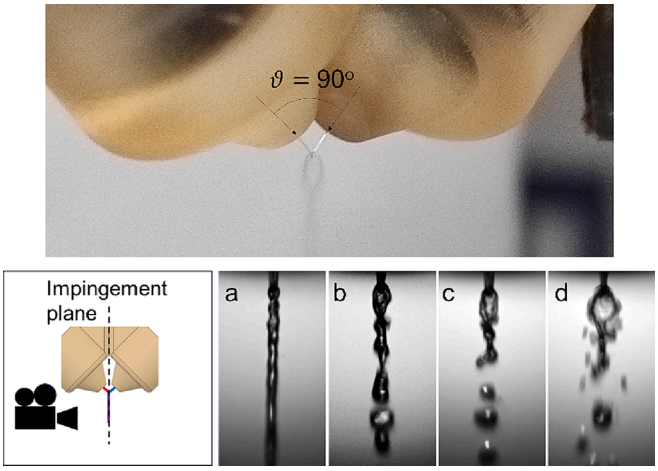

Fig. 3. Top: Photo of FIJR in operation at 3.30 ml/min per nozzle to showcase the liquid sheet formation. Bottom: High speed images (viewing angle normal to the impingement plane as indicated by camera icon) obtained for increasing flowrates. Information on flowrates and corresponding dimensionless numbers for cases a-d are provided in Table 1.

$$We_x = \frac{\rho \bullet (u \bullet \sin(\vartheta/2))^2 \bullet d}{\sigma} \tag{1}$$

where ρ is the fluid density, u is the average jet velocity magnitude, ϑ is the impingement angle, d is the jet diameter and σ is the fluid surface tension. Based on that, the We_x number calculated for the flow pattern in Fig. 3b, was close to the We_x providing the maximum mixing efficiency reported in previous work (Baber et al., 2016) (see Table 1). In addition, in flow patterns a, b and c, the outlet stream of the FIJR was directed downwards, making this range of flowrates appropriate for coupling the FIJR with a compact mCSTR, as the FIJR mixed stream can be accurately directed in an open tank.

3.3. Residence time distribution in the mCSTR cascade

Residence time distribution (RTD) has been shown to be of great importance for nanoparticle synthesis, directly affecting the particle size distribution (Panariello et al., 2018). The residence time distribution can be described by the $E(\theta)$ function, which in this work was calculated from the cumulative distribution (obtained with the step input) by direct numerical differentiation. The effect of the connecting tubes (inlet and outlet) was taken into consideration by subtracting the response obtained by the tubes only, via numerical Fast Fourier Transform (SI, section S3). The contribution was found negligible due to the short length and small volume of the connecting capillaries, and thus the system's $E(\theta)$ curves were used to assess the stirred tank cascade RTD. The numerical operations amplified the signal noise and thus required smoothening to produce smooth curves. An example of the numerical operations used to produce the $E(\theta)$ graphs is given in the SI, section S3. The experimental results are plotted together and compared with the ideal tanks-in-series model (Levenspiel, 1999) given by the equation:

$$E(\theta) = \frac{n(n\theta)^{n-1}}{(n-1)!}e^{-n\theta} \tag{2}$$

where n is the number of tanks in series, $\theta = t/\tau$ is the normalised time, t is the absolute time, $\tau = Q/V_r$ is the space time of the reactor (which for incompressible steady flow is equivalent to the theoretical mean residence time $t_{m,th}$), Q is the volumetric flow rate entering the reactor and V_r is the total free volume of the reactor (the volume occupied by the stir bars was subtracted). The fitting of the experimental data with the ideal tanks-in-series model was quantified by calculating the coefficient of determination, R^2:

$$R^2 = 1 - \frac{\sum_{\theta=0}^{4}\left(E(\theta)_{experimental} - E(\theta)_{tanks-in-series\ model}\right)^2}{\sum_{\theta=0}^{4}\left(E(\theta)_{experimental} - \overline{E}(\theta)_{experimental}\right)^2} \tag{3}$$

The summations are calculated from $\theta = 0$ to $\theta = 4$, as this is the range of the available experimental data.

The experimental mean residence time, t_m, was calculated from equation (4) (Levenspiel, 1999) as an additional means to evaluate deviation from ideal behaviour:

$$t_m = \tau \int_0^{\infty} \theta E(\theta) d\theta \tag{4}$$

The RTD calculation results for varying tank number are shown in Table 2.

RTD curves for a given flowrate (2 ml/min) and varying number of tanks (Fig. 4) show a good agreement with the ideal tanks-in-series model indicating a macromixing behaviour close to ideal mixing. Increasing the number of tanks led to the RTD becoming narrower and with the mode (peak of the distribution) moving closer to the theoretical mean residence time (t_m) as shown in Table 2, as expected from the ideal tanks-in-series model.

Discrepancies between the space time and the mean residence time can be attributed to 1) an effect of the open top (i.e., presence of a free liquid surface in the top tank), which allows the formation of a conical vortex, leading to slightly reduced liquid filled reactor volume, 2) the effect of the connecting tubes and reactor interconnections (causing a slight delay of the signal), and 3) effects of data processing which include error introduction via numerical differentiation (which is more significant at the edges of the dataset, i.e. $t = 0$) and the fact that the mean residence time was calculated via equation (4) using a finite integral from 0 to 4, as the experiments were run for time equivalent to 4x the space time as opposed to infinite time (leading to a smaller mean value, as observed). The worst agreement was observed for the single mCSTR, where all sources of error described above were more significant. The increase in the signal noise with increasing number of tanks can be attributed to a higher intensity of vibrations due to the simultaneous rotation of multiple stir bars. Despite the small discrepancies, the data indicated that only minor dead volumes existed between the tanks and negligible backmixing between the tanks occurred. In a preliminary design with multiple outlet ports, shown in the SI, section S6, this was not the case, as the multiple ports between the reactors created

Table 1
Reynolds, *Re*, Weber, *We*, and x-weighted Weber, We_x, number as a function of flowrate in the FIJR used in this work.

	a	*b*	*c*	*d*	*e**
Flowrate (ml/min)	1.68	2.16	2.46	3.3	15
Re	355	457	521	698	1269
We	17.4	28.8	37.3	67.2	88.8
We_x	8.7	14.3	18.7	33.6	14.7

*optimal mixing conditions reported in (Baber et al., 2016) using a FIJR with 0.25 mm ID nozzles in 48° angle.

Table 2
Residence time distribution metrics for varying tank number in the mCSTR cascade: reactor space time, $\tau = Q/V_r$, mean residence time, t_m, (equation (4)) and temporal position of the residence time distribution peak, RTD mode. Measurements are for 3 ml tanks with a 4.5 mm × 12 mm stir bar operating at 750 rpm and flowrate 2 ml/min (DI water at 20 °C).

Number of tanks	τ, total / per tank (s)	t_m, total / per tank (s)	RTD mode (s)
1	90 / 90	76.9 / 76.9	12.4
2	180 / 90	172.5 / 86.2	87.3
5	450 / 90	422.3 / 84.4	332.2

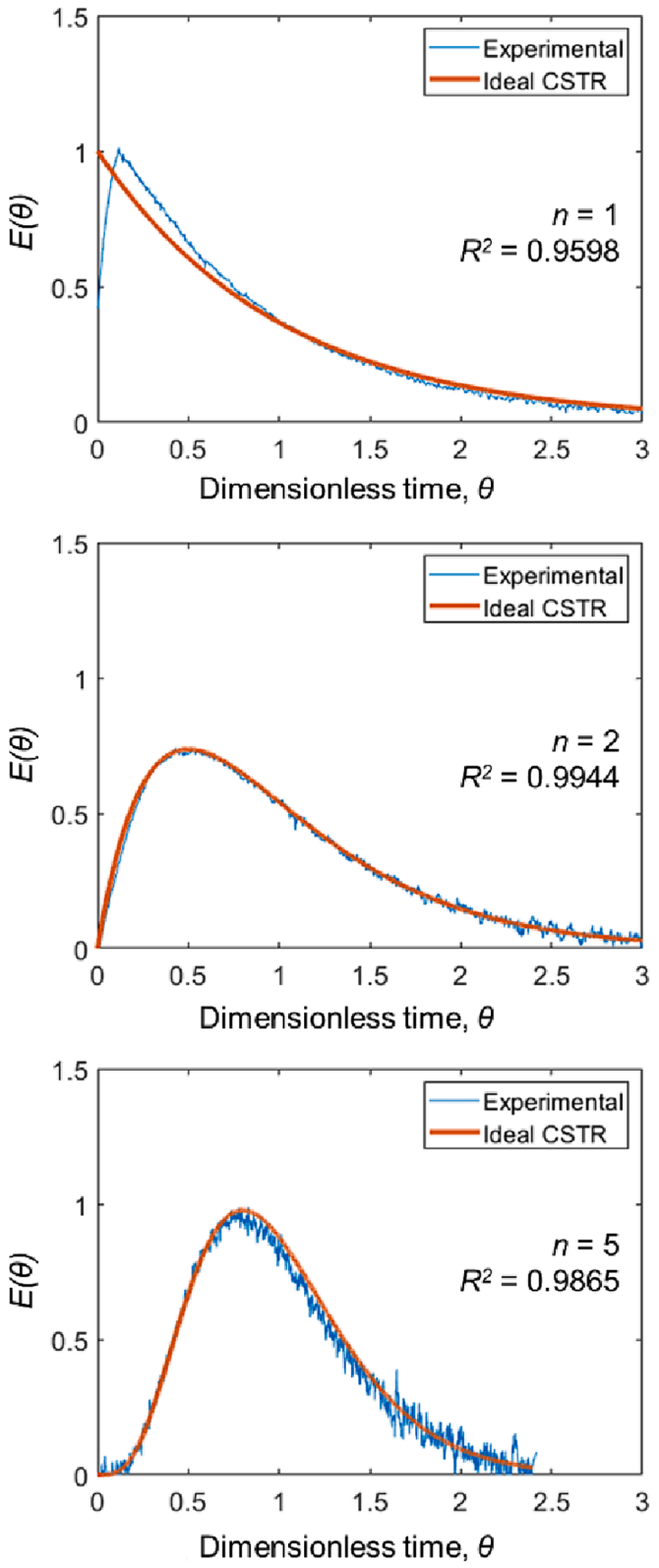

Fig. 4. Residence time distribution obtained for a varying number of mCSTRs, n (blue line) compared to the ideal tanks-in-series model (orange line). Measurements are for 3 ml tanks with a 4.5 mm × 12 mm stir bar operating at 750 rpm and flowrate 2 ml/min (DI water at 20 °C). The ideal CSTR curves were obtained from the tanks-in-series model.

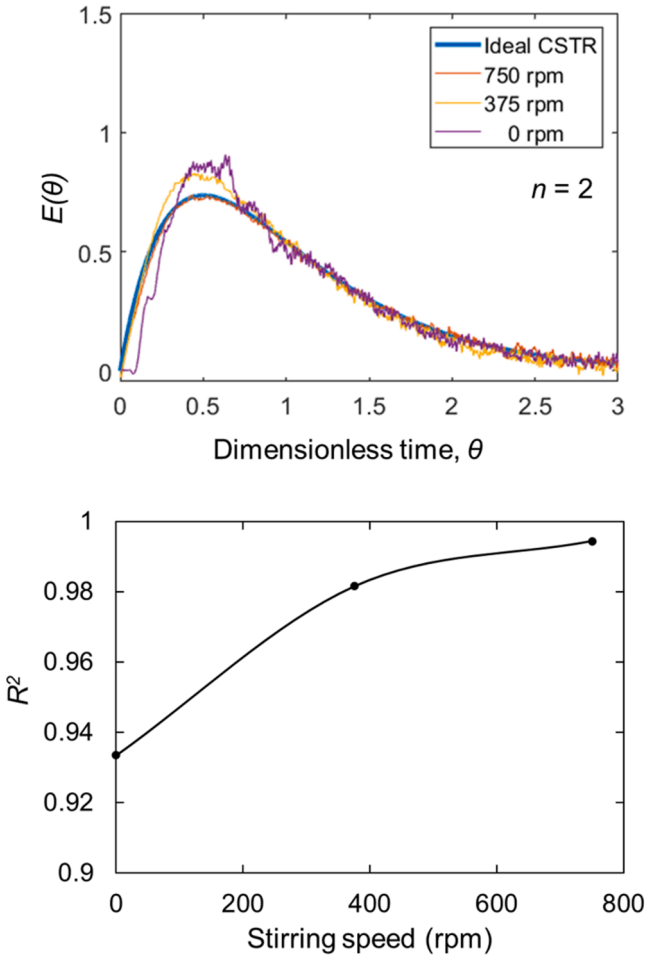

Fig. 5. Top: RTD of a two-mCSTR system operated at 2 ml/min for different stirring speeds. Measurements are for 3 ml tanks with a 4.5 mm × 12 mm stir bar (fluid was DI water at 20 °C). Bottom: Quantification of deviation from the ideal tanks-in-series model for varying stirring speed via the coefficient of determination (R^2). The ideal CSTR curve was obtained from the tanks-in-series model.

backmixing, leading to divergence from ideal behaviour.

The effect of stirring speed was tested in a two-mCSTR system run at 2 ml/min (Fig. 5). When no stirring was applied (the stir bar was present in the tank to maintain constant volume), an early peak of high intensity was observed (Fig. 5a), indicating a bypass (fluid moving from the inlet directly towards the outlet without being mixed with the rest of the tank volume) and the existence of dead volumes. The mixing behaviour increasingly approached the ideal CSTR with increasing the stirring speed (Fig. 5b). It should be noted that even without active stirring, the mixing behaviour was not far from the ideal CSTR ($R^2 \sim 0.93$) indicating that the kinetic energy of the inlet stream, combined with the confinement in the small tank can contribute to a significant mixing.

3.4. Nanoparticle synthesis

After assessing the hydrodynamics and RTD of the reactor system, it was used for two different colloidal nanoparticle synthesis case studies, both of which involved multiple steps. The particle quality, and potential issues with reactor operation (e.g., clogging) were investigated. Both nanoparticle synthesis experiments were performed at least twice to verify reproducibility in reactor operation.

3.4.1. Citrate-capped silver nanoparticles synthesis

Silver nanoparticles (AgNPs) were produced by the rapid reduction of $AgNO_3$ with a strong reductive agent ($NaBH_4$) in the presence of sodium citrate (which mainly promotes particle stabilisation), slightly adapting the protocols reported by (Agnihotri et al., 2014; Baber et al., 2016). An $AgNO_3$ solution was mixed rapidly with a solution containing $NaBH_4$ and sodium citrate in the FIJR part of the system, initiating the AgNP formation. The resulting solution was fed directly to the top, open mCSTR and then proceeded to the subsequent tanks, leaving the reactor system after an average residence time of ~ 3.75 min (2 ml/min per syringe, 5 x 3 ml mCSTRs) at 60 °C and under intense stirring (500 rpm). Preliminary work showed this reaction time to be suitable to obtain a colloidally stable product.

This synthesis is based on the co-reduction of Ag^+ via $NaBH_4$ and sodium citrate (Agnihotri et al., 2014) and involves multiple stages starting from the rapid initial formation of primary metallic silver nanoparticle seeds, followed by a slower growth stage and potential agglomeration/aggregation until eventually citrate ions stabilise silver nanoparticles by binding on their surface. The solution colour changed to an intense yellow even in the first mCSTR, indicating the production of AgNPs shortly after mixing (González et al., 2014). The particles were collected at the outlet of the reactor system as a colloidal dispersion that remained stable for at least 2 weeks after production. Fouling on the mCSTR walls was not visually observable after 50 min of operation (~200 ml of AgNP dispersion of 0.1 mM silver produced), even at the first mCSTRs where the reaction had not yet been completed. This was due to the wall-free initial mixing at the FIJR and the relatively low surface/volume ratio of the mCSTRs compared to common millifluidic or microfluidic tubular reactors.

The particle quality was evaluated via UV–Vis absorption, TEM, and DLS characterisation. The UV–Vis absorption spectrum of the Ag NPs dispersion was measured immediately (within 20 s) after the sample collection as well as 300 s, 600 s and 24 h after collection (Fig. 6a) showing only minor change (~5%) in the characteristic SPR peak intensity for silver nanoparticles within the first 5 min (the peak position remained the same). All the measurements after the 300 s timepoint were almost identical indicating good stability of the nanoparticles after collection without any post processing.

DLS showed an average hydrodynamic diameter of 20 nm (using the assumption of normal distribution). TEM imaging (Fig. 6b) showed well dispersed particles, and a small amount of two- or three-particle aggregates. The particle quality is comparable with previous reports (Baber et al., 2016; Sahoo and Kumar, 2021) in terms of particle size and polydispersity, proving the effectiveness of the proposed reactor combination for continuous AgNP synthesis. The particle size (obtained by TEM) is larger (9.2 ± 2.2 nm) compared to other syntheses utilising impinging jets such as (Baber et al., 2016) who used a similar protocol producing 5.9 ± 2.1 nm AgNPs or by (Sahoo and Kumar, 2021) who synthesised 5.4 ± 0.9 nm silver nanoparticles using tannic acid as reduction and capping agent. Using a coiled capillary reactor at similar temperature (60 °C), (Gao et al., 2022) produced smaller AgNPs of 4.3 ± 1.6 nm with a similar protocol. The polydispersity of the AgNPs produced with the FIJR × mCSTRs system, assessed via the coefficient of variation $\left(CoV = \frac{Standard\ deviation}{Average\ particle\ diameter}\right)$ was 23.9 %, which is in the same order as these similar syntheses described above (16 % – 34 %).

The difference in particle size can be attributed to variations in the experimental conditions. $NaBH_4$ has a stabilising effect early on AgNP synthesis when used in excess (Agnihotri et al., 2014; Zhang et al., 2011). In our work, this stabilising effect of $NaBH_4$ was limited as only a small quantity was used, potentially allowing particle growth via coalescence of smaller particles as described in (Polte et al., 2012). It should be noted that all other FIJR based syntheses of AgNPs (Baber et al., 2016; Sahoo and Kumar, 2021) were performed at room temperature whereas in the present reactor, the temperature was 60 °C. At elevated temperatures (60 °C – 90 °C), the nucleation of silver nanoparticles is accelerated more than growth, leading to smaller nanoparticle sizes (Casado et al., 2024). However, the balance between the nucleation, growth and stabilisation of silver nanoparticles can be affected by the chemical environment. A temperature increase has been shown to drive the silver nitrate reduction from $NaBH_4$ mediated, to citrate mediated (i.e. the reductive capacity of citrate increases with temperature) (Agnihotri et al., 2014; Gao et al., 2022). Specifically, at 60 °C a reduction of the [$NaBH_4$]/[citrate] ratio led to increase in nanoparticle size as a result of $NaBH_4$ primarily driving rapid nucleation, while citrate being mostly responsible for the formation of larger particles (Agnihotri et al., 2014). Thus, our significantly lower [$NaBH_4$]/[citrate] ratio may explain the larger particle size obtained in this work compared to

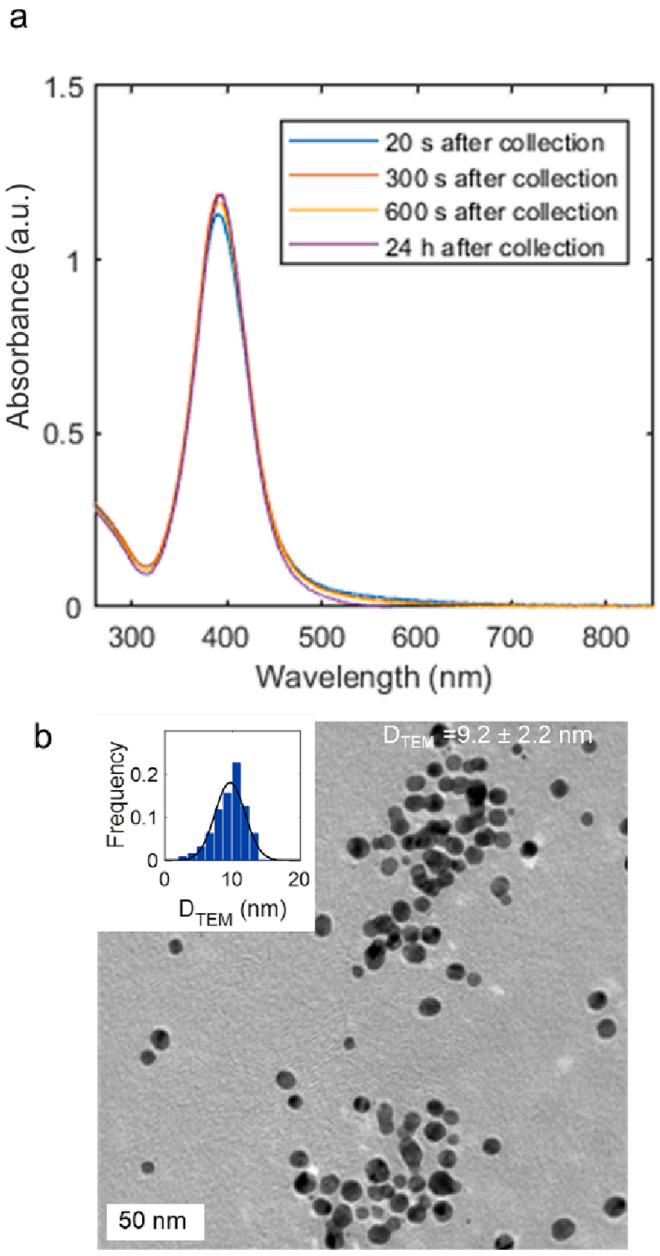

Fig. 6. Characterisation of silver nanoparticles produced with the FIJR - 5 × 3 ml mCSTRs system (60 °C, 3.75 min space time). a) UV–Vis spectra of sample collected at the outlet of the reactor system measured at 20, 300 and 600 s after collection and after 24 h of storage at ambient conditions. b) TEM image of silver nanoparticles with inset showing the particle size distribution (particle count, N = 185).

previously reported syntheses (Agnihotri et al., 2014; Baber et al., 2016; Gao et al., 2022; Sahoo and Kumar, 2021).

3.4.2. Magnetic iron oxide nanoparticles synthesis

The synthesis of IONPs was carried out in the same reactor system (5 × 3 ml mCSTRs). This synthesis was more challenging due to the higher solid content of the reactive stream, and the magnetic nature of the material which could potentially be affected by the magnetic field of the stir bars. Magnetite formation via coprecipitation and stabilisation by TEAOH has been reported in previous work (Gkogkos et al., 2022) to involve multiple steps including the initial particle formation, agglomeration in large visible flakes that may sediment, and deagglomeration by TEA^+ until a colloidally stable dispersion is formed. The temperature has also been reported as an important parameter for the synthesis, with higher temperatures leading to improved particle quality in terms of crystallinity and purity of magnetic product (Besenhard et al., 2021; Blanco-Andujar et al., 2012; Gkogkos et al., 2022). Following these previous reports, the temperature was set to 60 °C.

In the current reactor system, the initial particle formation occurred mid-air after rapidly mixing the iron precursor stream with the TEAOH solution stream in the FIJR operating at 2 ml/min for each stream, providing sufficient residence time for magnetite formation at 60 °C (Besenhard et al., 2020). The particles quickly formed agglomerates in the first tank (visible in the top, open tank) which deagglomerated going through the subsequent mCSTRs until a homogenous stream was obtained at the outlet of the reactor system. DLS analysis of the outlet stream directly after collection showed a ~80 nm particle size, proving the existence of colloidal nanoparticles and thus, the success of deagglomeration and stabilisation within the given reactor residence time.

The nanoparticles were additionally characterised via XRD and TEM. The XRD pattern (Fig. 7a) showed sharp peaks in good agreement with magnetite/maghemite peak positions suggesting that the produced nanoparticles were composed of magnetite or magnetite/maghemite mixture, as expected from the synthesis (Mascolo et al., 2013). While XRD cannot distinguish between magnetite and maghemite as they share a similar crystal structure, it is useful to verify that no additional, non-magnetic iron oxide crystals were produced.

TEM analysis (Fig. 7b) showed small and relatively monodisperse IONP cores of ~6.3 nm average size and CoV = 26.9 %, typical for an IONP co-precipitation synthesis. The size was slightly smaller compared to a similar synthetic process from previous work (8.6 nm) (Gkogkos et al., 2022) which could be explained by the superior initial mixing enabled by the FIJR compared to the predictable but slower diffusional mixing in the laminar flow device utilised in the above work. Batch synthesis using a similar protocol at room temperature (Mascolo et al., 2013) led to ~6.5 nm magnetite nanoparticles. In addition, (Siddiqui et al., 2009) demonstrated a co-precipitation synthesis of IONPs via a confined impinging jet reactor (CIJR) using various types of stabilising agents in the feed, producing nanoparticles ranging from 4.72 to 12.4 nm. The nanoparticles produced with the CIJR were in most cases more agglomerated compared to those produced with the reactor in the present work.

The results from TEM analysis differed from DLS (DLS size ~80 nm after synthesis), suggesting that the IONPs exist as small, stabilised agglomerates (as also suggested in the literature (Mascolo et al., 2013)). Deagglomeration continued even after collection, but at a much slower rate (remeasuring the samples after 2 weeks the DLS particle size was found to have dropped to ~40 nm). To further improve the stability of the nanoparticles, the synthesis process was split in two parts featuring an initial reaction step using the FIJR × mCSTR cascade at room temperature (~3.75 min mean residence time). Measuring the hydrodynamic diameter directly after the FIJR × mCSTR cascade operating at room temperature led to a size of ~20 nm indicating greatly improved stabilisation. For the two-step process, the FIJR × mCSTR cascade operating at room temperature was followed by a subsequent step at a coiled capillary reactor operated at 60 °C (additional 4 min residence

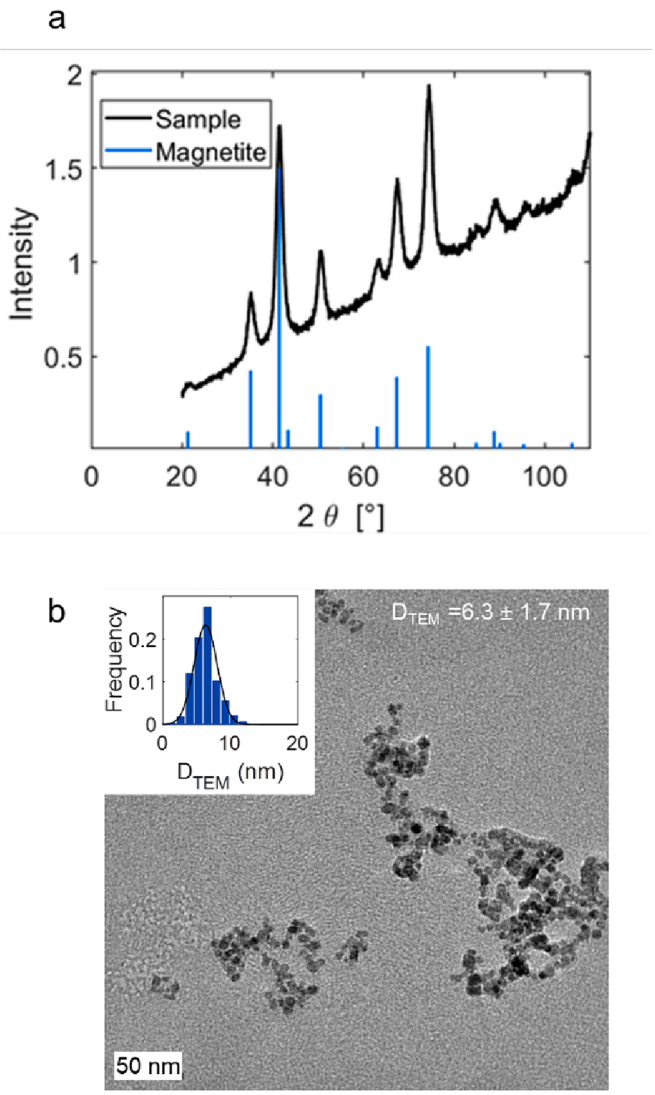

Fig. 7. Characterisation of iron oxide nanoparticles (IONPs) produced with the FIJR – 5 × 3 ml mCSTRs system (60 °C, 3.75 min space time). a) XRD pattern showcasing the peaks of magnetite/maghemite (PDF® reference: 03–065-3107), b) TEM image of IONPs with inset showing the particle size distribution (particle count, N = 210).

time) to accelerate the transformation of intermediate iron oxide phases to magnetite (Blanco-Andujar et al., 2012) and prevent the existence of impurities in the outlet stream. It should be noted that the reaction could be completed entirely at room temperature given adequate residence time (Mascolo et al., 2013). The nanoparticle quality, as characterised by TEM and XRD was similar to the 60 °C single step synthesis (the TEM is shown in SI, section S7). However, the hydrodynamic diameter of the nanoparticles as measured by DLS was ~16 nm which is closer to the TEM average size of ~6.1 nm indicating an improved deagglomeration behaviour when the first steps of the synthetic process take place at room temperature.

In both cases (single and two-step process) the reactor system was operated continuously for over 2 h without clogging despite the high particle load. Fluid retention was evaluated by monitoring the level of the top open stirred tank. At steady state the level should not change whereas significant particle accumulation or clogging would lead to rapid overfill. After operation, the reactor system was cleared of particles successfully when the reactant streams were changed to DI water. While no significant fouling was observed on the reactor walls, in the single step process, some particle accumulation was observed on the

magnetic poles of the stir bars. This may lead to problems when the reactor system is operated for prolonged periods. However, since these are areas of maximum fluid velocity (and thus shear), accumulation of enough material to disrupt the process is considered unlikely, as evident from the limited fouling during the 2 h operation. Interestingly, in the two-step process particle accumulation was significantly reduced, and limited on the stir bar in the top mCSTR where the stabilization process had not been completed.

The temperature dependent behaviour described above can be attributed to the competition between multiple steps that may occur after nanoparticle formation. Assuming a rapid nanoparticle formation due to enhanced mixing in the FIJR, the nanoparticles may interact with each other, forming agglomerates, or with the stabilising agent (TEA^+) to become colloidally stable, with these processes taking place simultaneously. A higher temperature is generally known to accelerate agglomeration phenomena by increasing the probability of particle–particle collision (Wang et al., 2021) while it may also affect the interaction of TEA^+ with the IONP surface and thus, the stabilisation process. Furthermore, an increase in temperature may affect the agglomeration process by reducing the viscosity of a Newtonian fluid solvent, leading to weaker shear stress induced by a stir bar operating at specific stirring speed and eventually alteration of the agglomeration rate (Lv et al., 2016).

4. Conclusions

This work has presented the design, evaluation and application of a reactor system purpose built to produce colloidal nanoparticles that involve multiple stages that occur at different timescales. Rapid mixing is guaranteed by using a FIJR which feeds directly into a cascade of mCSTRs which provides the required residence time and temperature management for the rest of the synthesis. The mCSTR cascade was arranged in a compact vertical configuration facilitating stirring and heating with a single stirrer/hotplate, and minimising interconnections. The design for 3D printing of most reactor modules makes the device easy to manufacture and allows rapid deployment in a lab environment, which, in combination with the similar to batch reactor hydrodynamics, may allow faster transition from batch to continuous flow nanomaterial synthesis development. The main limitation required to be overcome lies in the magnetic coupling between the stir bars, since the magnetic field of the stirrer can support a maximum of 6 simultaneously operating stages (5 mCSTRs + 1 stir bar for the stirred heating bath) while the attraction between the stir bars limits the minimum height of the tanks (and thus the volume for a given residence time). Characterisation of the reactor system revealed the operating regime (flowrates) for rapid mixing with the FIJR, and a near-ideal behaviour of the mCSTR cascade in terms of mixing, with good temperature control.

The reactor system's effectiveness was verified by two individual case studies of nanomaterial synthesis. Both the AgNP and the IONP syntheses produced small and relatively monodisperse nanoparticles. Stable colloidal suspensions were collected at the outlet of the reactor system, indicating that the mCSTR cascade provided good control of the residence time distribution, without suffering from fouling and particle settling. In addition, the IONP synthesis provided valuable insights on the reactor operation, especially regarding the interaction of the stir bars with magnetic particles. While some agglomerated particles were found on the magnetic stir bars, this did not interrupt the normal operation of the reactor. Furthermore, coupling the FIJR × mCSTRs system with a second coil reactor, led to less agglomerated IONPs by performing the initial mixing/particle formation at a lower temperature, underlining the advantage of flow systems for multistage processes.

CRediT authorship contribution statement

Georgios Gkogkos: Data curation, Formal analysis, Investigation, Methodology, Software, Visualization, Writing – original draft, Writing – review & editing. **Liudmyla Storozhuk:** Investigation. **Jacopo Piovesan:** Methodology. **Mathew R. Penny:** Methodology, Investigation, Conceptualization. **Stephen T. Hilton:** Writing – review & editing, Resources. **Nguyen Thi Kim Thanh:** Writing – review & editing, Resources, Funding acquisition. **Asterios Gavriilidis:** Writing – review & editing, Supervision, Resources, Project administration, Methodology, Funding acquisition.

Declaration of competing interest

The authors declare that they have no known competing financial interests or personal relationships that could have appeared to influence the work reported in this paper.

Data availability

Data will be made available on request.

Acknowledgments

We thank Dr. Alaric Taylor for useful discussions regarding the initial design of the reactor tanks and Dr. Sayan Pal for advice on high-speed imaging. We thank the EPSRC (EP/M015157/1) through the Manufacturing Advanced Functional Materials (MAFuMa) scheme for financial support. Georgios Gkogkos is grateful to the Hugh Walter Stern PhD studentship for his funding.

Appendix A. Supplementary data

Supplementary data to this article can be found online at https://doi.org/10.1016/j.ces.2024.120081.

References

Abiev, R.S., Sirotkin, A.A., 2020. Influence of hydrodynamic conditions on micromixing in microreactors with free impinging jets. Fluids 5, 179. https://doi.org/10.3390/fluids5040179.

Abou-Hassan, A., Bazzi, R., Cabuil, V., 2009a. Multistep continuous-flow microsynthesis of magnetic and fluorescent γ-Fe2O3 @SIO2 core/shell nanoparticles. Angew. Chem. 121, 7316–7319. https://doi.org/10.1002/ange.200902181.

Abou-Hassan, A., Sandre, O., Neveu, S., Cabuil, V., 2009b. Synthesis of goethite by separation of the nucleation and growth processes of ferrihydrite nanoparticles using microfluidics. Angew. Chem. Internat. Ed. 48, 2342–2345. https://doi.org/10.1002/anie.200805933.

Agnihotri, S., Mukherji, S., Mukherji, S., 2014. Size-controlled silver nanoparticles synthesized over the range 5–100 nm using the same protocol and their antibacterial efficacy. RSC Adv. 4, 3974–3983. https://doi.org/10.1039/c3ra44507k.

Albadi, Y., Sirotkin, A.A., Semenov, V.G., Abiev, R.S., Popkov, V.I., 2020. Synthesis of superparamagnetic $GdFeO_3$ nanoparticles using a free impinging-jets microreactor. Russ. Chem. Bull. 69, 1290–1295. https://doi.org/10.1007/s11172-020-2900-x.

Asimakidou, T., Makridis, A., Veintemillas-Verdaguer, S., Morales, M.P., Kellartzis, I., Mitrakas, M., Vourlias, G., Angelakeris, M., Simeonidis, K., 2020. Continuous production of magnetic iron oxide nanocrystals by oxidative precipitation. Chem. Eng. J. 393, 124593 https://doi.org/10.1016/j.cej.2020.124593.

Baber, R., Mazzei, L., Thanh, N.T.K., Gavriilidis, A., 2016. Synthesis of silver nanoparticles using a microfluidic impinging jet reactor. J. Flow Chem. 6, 268–278. https://doi.org/10.1556/1846.2016.00015.

Besenhard, M.O., Baber, R., LaGrow, A.P., Mazzei, L., Thanh, N.T.K., Gavriilidis, A., 2018. New insight into the effect of mass transfer on the synthesis of silver and gold nanoparticles. CrystEngComm 20, 7082–7093. https://doi.org/10.1039/C8CE01014E.

Besenhard, M.O., LaGrow, A.P., Hodzic, A., Kriechbaum, M., Panariello, L., Bais, G., Loizou, K., Damilos, S., Margarida Cruz, M., Thanh, N.T.K., Gavriilidis, A., 2020. Co-precipitation synthesis of stable iron oxide nanoparticles with NaOH: New insights and continuous production via flow chemistry. Chem. Eng. J. 399, 125740 https://doi.org/10.1016/j.cej.2020.125740.

Besenhard, M.O., Panariello, L., Kiefer, C., Lagrow, A.P., Storozhuk, L., Perton, F., Begin, S., Mertz, D., Thanh, N.T.K., Gavriilidis, A., 2021. Small iron oxide nanoparticles as MRI T_1 contrast agent: Scalable inexpensive water-based synthesis using a flow reactor. Nanoscale 13, 8795–8805. https://doi.org/10.1039/d1nr00877c.

Besenhard, M.O., Pal, S., Gkogkos, G., Gavriilidis, A., 2023. Non-fouling flow reactors for nanomaterial synthesis. React. Chem. Eng. 8, 955–977. https://doi.org/10.1039/d2re00412g.

Blanco-Andujar, C., Ortega, D., Pankhurst, Q.A., Thanh, N.T.K., 2012. Elucidating the morphological and structural evolution of iron oxide nanoparticles formed by

sodium carbonate in aqueous medium. J. Mater. Chem. 22, 12498–12506. https://doi.org/10.1039/c2jm31295f.
Casado, C., Pinho, B., Marugán, J., Torrente-Murciano, L., 2024. Predicting the size of silver nanoparticles synthesised in flow reactors: Coupling population balance models with fluid dynamic simulations. Chem. Eng. J. 479, 147684 https://doi.org/10.1016/J.CEJ.2023.147684.
Chapman, M.R., Kwan, M.H.T., King, G., Jolley, K.E., Hussain, M., Hussain, S., Salama, I. E., González Nino, C., Thompson, L.A., Bayana, M.E., Clayton, A.D., Nguyen, B.N., Turner, N.J., Kapur, N., Blacker, A.J., 2017. Simple and versatile laboratory scale CSTR for multiphasic continuous-flow chemistry and long residence times. Org. Process Res. Dev. 21, 1294–1301. https://doi.org/10.1021/acs.oprd.7b00173.
Chen, Q., Deng, J., Luo, G., 2023. Micromixing performance and residence time distribution in a miniaturized magnetic reactor: Experimental investigation and machine learning modeling. Ind. Eng. Chem. Res. 62, 3577–3591. https://doi.org/10.1021/acs.iecr.2c04513.
Cherkasov, N., Adams, S.J., Bainbridge, E.G.A., Thornton, J.A.M., 2022. Continuous stirred tank reactors in fine chemical synthesis for efficient mixing, solids-handling, and rapid scale-up. React. Chem. Eng. 8, 266–277. https://doi.org/10.1039/d2re00232a.
Clanet, C., Lasheras, J.C., 1999. Transition from dripping to jetting. J. Fluid Mech. 383, 307–326. https://doi.org/10.1017/S0022112098004066.
Damilos, S., Alissandratos, I., Panariello, L., Radhakrishnan, A.N.P., Cao, E., Wu, G., Besenhard, M.O., Kulkarni, A.A., Makatsoris, C., Gavriilidis, A., 2021. Continuous citrate-capped gold nanoparticle synthesis in a two-phase flow reactor. J. Flow Chem. 11, 553–567. https://doi.org/10.1007/s41981-021-00172-3.
Deshpande, J.B., Kulkarni, A.A., 2018. Reaction engineering for continuous production of silver nanoparticles. Chem. Eng. Technol. 41, 157–167. https://doi.org/10.1002/ceat.201700035.
Erni, P., Elabbadi, A., 2013. Free impinging jet microreactors: Controlling reactive flows via surface tension and fluid viscoelasticity. Langmuir 29, 7812–7824. https://doi.org/10.1021/la401017z.
Gao, Y., Pinho, B., Torrente-Murciano, L., 2022. Tailoring the size of silver nanoparticles by controlling mixing in microreactors. Chem. Eng. J. 432, 134112 https://doi.org/10.1016/j.cej.2021.134112.
Gkogkos, G., Besenhard, M.O., Storozhuk, L., Thanh, N.T.K., Gavriilidis, A., 2022. Fouling-proof triple stream 3D flow focusing based reactor: Design and demonstration for iron oxide nanoparticle co-precipitation synthesis. Chem. Eng. Sci. 251, 117481 https://doi.org/10.1016/j.ces.2022.117481.
González, A.L., Noguez, C., Beránek, J., Barnard, A.S., 2014. Size, shape, stability, and color of plasmonic silver nanoparticles. J. Phys. Chem. C 118, 9128–9136. https://doi.org/10.1021/JP5018168.
Jolivet, J.P., Chanéac, C., Tronc, E., 2004. Iron oxide chemistry. From molecular clusters to extended solid networks. Chem. Commun. 4, 477–483. https://doi.org/10.1039/b304532n.
Kumar, D.V.R., Prasad, B.L.V., Kulkarni, A.A., 2013. Impinging jet micromixer for flow synthesis of nanocrystalline MgO: Role of mixing/impingement zone. Ind. Eng. Chem. Res. 52, 17376–17382. https://doi.org/10.1021/ie402012x.
Levenspiel, O., 1999. Chemical Reaction Engineering, 3rd ed. John Wiley & Sons, Inc, New York.
Li, R., Ashgriz, N., 2006. Characteristics of liquid sheets formed by two impinging jets. Phys. Fluids 18, 087104. https://doi.org/10.1063/1.2338064.
Lignos, I., Ow, H., Lopez, J.P., McCollum, D., Zhang, H., Imbrogno, J., Shen, Y., Chang, S., Wang, W., Jensen, K.F., 2020. Continuous multistage synthesis and functionalization of sub-100 nm silica nanoparticles in 3D-printed continuous stirred-tank reactor cascades. ACS Appl. Mater. Interfaces 12, 6699–6706. https://doi.org/10.1021/acsami.9b20605.
Lignos, I., Mo, Y., Carayannopoulos, L., Ginterseder, M., Bawendi, M.G., Jensen, K.F., 2021. A high-temperature continuous stirred-tank reactor cascade for the multistep synthesis of InP/ZnS quantum dots. React. Chem. Eng. 6, 459–464. https://doi.org/10.1039/d0re00454e.
Lv, B., Wang, C., Hou, J., Wang, P., Miao, L., Li, Y., Ao, Y., Yang, Y., You, G., Xu, Y., 2016. Influence of shear forces on the aggregation and sedimentation behavior of cerium dioxide (CeO2) nanoparticles under different hydrochemical conditions. J. Nanopart. Res. 18, 1–12. https://doi.org/10.1007/s11051-016-3501-3.
Mascolo, M.C., Pei, Y., Ring, T.A., 2013. Room temperature co-precipitation synthesis of magnetite nanoparticles in a large pH window with different bases. Materials 6, 5549–5567. https://doi.org/10.3390/ma6125549.
McNamara, K., Tofail, S.A.M., 2017. Nanoparticles in biomedical applications. Adv. Phys. X 2, 54–88. https://doi.org/10.1080/23746149.2016.1254570.
Mittal, D., Kaur, G., Singh, P., Yadav, K., Ali, S.A., 2020. Nanoparticle-based sustainable agriculture and food science: Recent advances and future outlook. Front. Nanotechnol. 2, 579954. https://doi.org/10.3389/fnano.2020.579954.
Mo, Y., Jensen, K.F., 2016. A miniature CSTR cascade for continuous flow of reactions containing solids. React. Chem. Eng. 1, 501–507. https://doi.org/10.1039/c6re00132g.
Narayan, N., Meiyazhagan, A., Vajtai, R., 2019. Metal nanoparticles as green catalysts. Materials 12, 3602. https://doi.org/10.3390/ma12213602.
Panariello, L., Mazzei, L., Gavriilidis, A., 2018. Modelling the synthesis of nanoparticles in continuous microreactors: The role of diffusion and residence time distribution on nanoparticle characteristics. Chem. Eng. J. 350, 1144–1154. https://doi.org/10.1016/j.cej.2018.03.167.
Panariello, L., Wu, G., Besenhard, M.O., Loizou, K., Storozhuk, L., Thanh, N.T.K., Gavriilidis, A., 2020. A modular millifluidic platform for the synthesis of iron oxide nanoparticles with control over dissolved gas and flow configuration. Materials 13, 1019. https://doi.org/10.3390/ma13041019.
Pathakoti, K., Manubolu, M., Hwang, H.M., 2018. Nanotechnology applications for environmental industry. Handbook of Nanomaterials for Industrial Applications, Chap. 48 894–907. https://doi.org/10.1016/B978-0-12-813351-4.00050-X.
Phan, H.T., Haes, A.J., 2019. What does nanoparticle stability mean? J. Phys. Chem. C 123, 16495–16507. https://doi.org/10.1021/acs.jpcc.9b00913.
Pinho, B., Torrente-Murciano, L., 2020. Continuous manufacturing of silver nanoparticles between 5 and 80 nm with rapid online optical size and shape evaluation. React. Chem. Eng. 5, 342–355. https://doi.org/10.1039/c9re00452a.
Polte, J., Tuaev, X., Wuithschick, M., Fischer, A., Thuenemann, A.F., Rademann, K., Kraehnert, R., Emmerling, F., 2012. Formation mechanism of colloidal silver nanoparticles: analogies and differences to the growth of gold nanoparticles. ACS Nano 6, 5791–5802. https://doi.org/10.1021/nn301724z.
Proskurina, O.V., Sivtsov, E.V., Enikeeva, M.O., Sirotkin, A.A., Abiev, R.Sh., Gusarov, V. V., 2019. Formation of rhabdophane-structured lanthanum orthophosphate nanoparticles in an impinging-jets microreactor and rheological properties of sols based on them. Nanosyst. Phys. Chem. Math. 10, 206–214. https://doi.org/10.17586/2220-8054-2019-10-2-206-214.
Rossi, D., Gargiulo, L., Valitov, G., Gavriilidis, A., Mazzei, L., 2017. Experimental characterization of axial dispersion in coiled flow inverters. Chem. Eng. Res. Des. 120, 159–170. https://doi.org/10.1016/j.cherd.2017.02.011.
Sahoo, K., Kumar, S., 2021. Green synthesis of sub 10 nm silver nanoparticles in gram scale using free impinging jet reactor. Chem. Eng. Process. - Process Intesif. 165, 108439 https://doi.org/10.1016/j.cep.2021.108439.
Siddiqui, S.W., Unwin, P.J., Xu, Z., Kresta, S.M., 2009. The effect of stabilizer addition and sonication on nanoparticle agglomeration in a confined impinging jet reactor. Colloids Surf. A Physicochem. Eng. Asp. 350, 38–50. https://doi.org/10.1016/j.colsurfa.2009.08.031.
Tacsi, K., Joó, Á., Pusztai, É., Domokos, A., Nagy, Z.K., Marosi, G., Pataki, H., 2021. Development of a triple impinging jet mixer for continuous antisolvent crystallization of acetylsalicylic acid reaction mixture. Chem. Eng. Process. - Process Intesif. 165, 1–11. https://doi.org/10.1016/j.cep.2021.108446.
Wang, J., Li, Z., Jia, Y., Wang, B., Xu, Z., 2021. Molecular dynamics simulation of effect of temperature on Cu nanoparticles agglomeration of nanofluids. J. Nanopart. Res. 23, 28. https://doi.org/10.1007/s11051-020-05131-y.
Zhang, Q., Li, N., Goebl, J., Lu, Z., Yin, Y., 2011. A systematic study of the synthesis of silver nanoplates: Is citrate a “magic” reagent? J. Am. Chem. Soc. 133, 18931–18939. https://doi.org/10.1021/ja2080345.